Beyond the creeping viscous flow limit for lipid bilayer membranes: Theory of single-particle microrheology, domain flicker spectroscopy, and long-time tails

Brian A. Camley[1] and Frank L. H. Brown[2,1]
[1]*Department of Physics, University of California, Santa Barbara, California 93106, USA*
[2]*Department of Chemistry and Biochemistry, University of California, Santa Barbara, California 93106, USA*
(Received 6 May 2011; published 4 August 2011)

Recent experiments suggest that lipid bilayer membranes may be viscoelastic. We present a generalized "Saffman-Einstein" relation that may be used to determine the linear viscoelastic shear modulus from single-bead microrheology experiments on membranes. We show that viscoelastic parameters can also be extracted from membrane domain flicker spectroscopy experiments. Contributions from fluid inertia are expected to be negligible in both microrheology and domain flicker spectroscopy experiments, but can create a "long-time tail" in the membrane velocity autocorrelation function. In a viscous membrane, this tail crosses over from t^{-1} at intermediate times, as in a two-dimensional fluid, to $t^{-3/2}$ at long times, as in a three-dimensional fluid. If the membrane is viscoelastic, the velocity autocorrelation function may be negative at intermediate times.

DOI: 10.1103/PhysRevE.84.021904 PACS number(s): 87.16.dm, 83.60.Bc, 83.10.Mj

Hydrodynamic theories of "quasi-two-dimensional" fluids, i.e., two-dimensional fluids surrounded by a bulk, three-dimensional fluid, have been remarkably successful in describing the dynamic behavior of membranes [1–6], interfaces [7,8], lipid monolayers [9], and liquid crystals [10]. Recent microrheology experiments have indicated that membranes may have viscoelastic properties with crossover between viscous and elastic behavior at times in the range of 10–100 ms [11]. Classical measurements of the membrane surface viscosity [12] do not address the potential frequency dependence of viscosity. Other experiments suggest that the crossover time scale should be approximately 50 μs [13], or less than 100 ms [14], if the membrane is above its melting temperature.

Past analysis of the diffusion of lipid domains [3,4], as well as "domain flicker spectroscopy" [15,16] and phase separation [6], have assumed that the membrane is purely viscous. In this paper, we extend previously developed results for purely viscous quasi-two-dimensional fluids to viscoelastic membranes, deriving formulas for both the mobility of embedded objects and the relaxation of distorted domains. We also extend this treatment to include the inertia of both the membrane and the surrounding bulk fluid, allowing us to predict long-time tails in the membrane velocity autocorrelation function.

Many theoretical tools have been developed to treat the hydrodynamics of quasi-two-dimensional viscous membranes [2,5,17] in the creeping-flow limit, and some work has been done on expressly viscoelastic membranes [18]. The well-known correspondence between viscous creeping flows and linear viscoelastic flows [19] allows us to transform solutions to the viscous problem into those for the viscoelastic one, simply by transforming into frequency space and replacing the viscosity η with a complex, frequency-dependent viscosity $\eta(\omega)$. One-particle microrheology uses this correspondence to measure linear viscoelastic properties of a homogeneous medium by using a generalized Stokes-Einstein formula [20].

We treat the membrane as a two-dimensional continuum surrounded by a bulk fluid. This approach has been remarkably successful in describing the deformations of the membrane surface, both in terms of equilibrium shape [21,22] and fluctuations around it [23,24] as well as the dynamics of membrane height fluctuations [25–27]. We focus on fluid motion within the bilayer, which is to linear order decoupled from deformations of the bilayer [18]. We therefore describe the membrane as a two-dimensional fluid embedded within a three-dimensional bulk fluid (Fig. 1), a model most prominently used by Saffman and Delbrück [1]. If the membrane is purely viscous, we can solve the Stokes equations for the coupled membrane-bulk fluid system with a force distribution $\mathbf{f}(\mathbf{r},t)$ by using a Green's function technique [5,17,28]; the membrane velocity is given by

$$v_m^i(\mathbf{k},\omega) = T^{ij}(\mathbf{k},\omega) f^j(\mathbf{k},\omega), \tag{1}$$

where the Einstein summation convention is assumed. The force $\mathbf{f}$ and the membrane velocity $\mathbf{v}_m$ vectors are within the membrane plane; our convention is $\mathbf{f}(\mathbf{k},\omega) = \int d^2r\, dt\, e^{-i(\mathbf{k}\cdot\mathbf{r}+\omega t)}\mathbf{f}(\mathbf{r},t)$. We will refer to $T^{ij}(\mathbf{k},\omega)$ as the "membrane Oseen tensor," in analogy with the similar tensor for pure fluids [29]. $T^{ij}(\mathbf{k},\omega)$ is well known in the limit of a purely viscous, incompressible membrane at small Reynolds number (the "creeping flow" limit) [5,17,18],

$$T^{ij}(\mathbf{k},\omega) = \frac{\delta_{ij} - k_i k_j/k^2}{\eta_m k^2 + 2\eta_f k} \quad \text{(creeping viscous flow)}, \tag{2}$$

where η_m is the surface viscosity of the membrane and η_f is the viscosity of the bulk fluid surrounding it. In Appendix A, we derive a generalized form of the membrane Oseen tensor that describes an incompressible, linear viscoelastic membrane at small Reynolds number, including the membrane and bulk fluid inertia. This result is

$$T^{ij}(\mathbf{k},\omega) = \frac{\delta_{ij} - k_i k_j/k^2}{i\omega\rho_m + \eta_m(\omega)k^2 + 2\eta_f k\sqrt{1 + i\omega/\omega_f(k)}}, \tag{3}$$

where $\eta_m(\omega)$ is the complex surface viscosity, ρ_m is the two-dimensional membrane mass density, ρ_f is the bulk fluid density, and $\omega_f(k) = \eta_f k^2/\rho_f$. A similar membrane Oseen tensor has also been derived for a purely viscous membrane [28]. Equation (3) reduces to Eq. (2) in the limit of $\omega \to 0$.

We present three applications of the generalized membrane Oseen tensor, Eq. (3), to physical problems: (i) determining

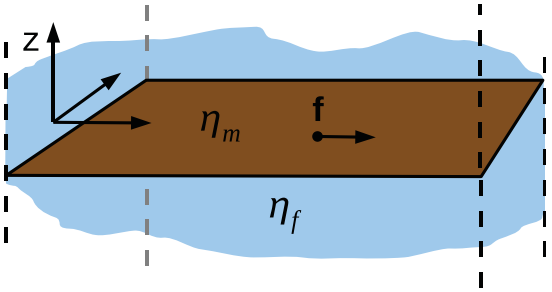

FIG. 1. (Color online) A quasi-two-dimensional membrane: a two-dimensional fluid with complex surface viscosity $\eta_m(\omega)$ surrounded by a bulk fluid with viscosity η_f. All forces $\mathbf{f}$ applied are within the plane of the membrane.

viscoelastic moduli from single-particle mean-squared displacements in a membrane, (ii) determining viscoelastic parameters from domain flickering in multicomponent membranes, and (iii) calculating the long-time tails in membrane velocity autocorrelation functions, which are due to membrane and bulk fluid inertia.

I. SINGLE-PARTICLE MICRORHEOLOGY IN A MEMBRANE

Single-particle microrheology relates the thermal fluctuations of a tracer particle to the linear viscoelastic properties of the material surrounding it through a generalized Stokes-Einstein equation [20]. The Einstein relationship between the particle mean-squared displacement and its mobility holds for an isotropic membrane if the tracer particle is large enough that the membrane can reasonably be approximated as a homogeneous continuum. With this assumption, the fluctuation-dissipation theorem implies that [30]

$$\zeta(\omega) = \frac{2Nk_BT}{(i\omega)^2\mathcal{F}_u\{\langle\Delta\mathbf{r}^2(t)\rangle\}(\omega)}, \tag{4}$$

where N is the number of degrees of freedom tracked in the mean-squared displacement and $\mathcal{F}_u\{g(t)\}(\omega) \equiv \int_0^\infty g(t)e^{-i\omega t}$ is the unilateral Fourier transform (or "Fourier-Laplace" transform). $\zeta(\omega)$ here is the hydrodynamic resistance [20], i.e., if a particle has an oscillating velocity $\mathbf{v}_p(\omega)$, the hydrodynamic drag on the particle is $\mathbf{F}_D = -\zeta(\omega)\mathbf{v}_p(\omega)$. Equivalently, $\zeta(\omega)$ is the inverse of the complex mobility, $\mu(\omega)$, $\mathbf{v}_p(\omega) = \mu(\omega)\mathbf{F}(\omega)$, where $\mathbf{F}(\omega)$ is an external force applied to the particle [20].

In bulk microrheology, the mean-squared displacements are analyzed by assuming the Stokes formula for ζ, i.e., $\zeta(\omega) = 6\pi\eta(\omega)a$, where a is the particle radius. This is not the appropriate formula for membranes; instead, ζ is given by a more complicated form derived initially by Saffman and Delbrück [1] and extended by Hughes, Pailthorpe, and White [2]:

$$\zeta = 4\pi\eta_m Z(a/L_{\mathrm{SD}}), \tag{5}$$

where $Z(x) \to 1/[\ln(2/x) - \gamma_E]$ for $x \ll 1$ and $Z(x) \to 2x/\pi$ for $x \gg 1$, where L_{SD} is the Saffman-Delbrück length, $L_{\mathrm{SD}} = \eta_m/2\eta_f$, and $\gamma_E = 0.5772\ldots$ is the Euler-Mascheroni constant. Naively, we could write a "generalized Saffman-Einstein relation" simply by choosing the relevant limit, and replacing η_m in this formula with $\eta_m(\omega)$. However, even for a small tracer particle, $a \ll L_{\mathrm{SD}}(\omega = 0)$, both limits may be relevant if $\eta_m(\omega)$ significantly decreases at any frequency. An interpolation formula for $f(x)$ has been derived [4], but applying an analytical continuation like $\eta_m \to \eta_m(\omega)$ to an interpolation seems ill-founded; similar concerns apply to the complex numerical scheme used in [2].

Instead of directly solving the complicated boundary value problem as in [2], we introduce an immersed-boundary (IB) approximation [31,32] for the particle-fluid coupling, which yields

$$\zeta^{-1}(\omega) = \frac{1}{4\pi}\int_0^\infty dk \frac{ke^{-\beta^2k^2a^2/2}}{i\omega\rho_m + \eta_m(\omega)k^2 + 2\eta_f k\sqrt{1 + i\omega/\omega_f(k)}}, \tag{6}$$

where $\beta = 0.797\,91$ (see Appendix B for details). Similar forms may be derived by using the methods of Levine, Mackintosh, and Lubensky [18,33], e.g., the "shell localization" scheme of [33]), and these provide qualitatively similar results (see Appendix C). Immersed boundary methods have also been used to calculate mobilities [32,34] and long-time tails [32,35] for particles in ordinary three-dimensional fluids.

Using this formula, mean-squared displacement data $\langle\Delta\mathbf{r}^2(t)\rangle$ can be analyzed by determining $\zeta(\omega)$ from the Einstein relation, Eq. (4), as in [30]. Then $\eta_m(\omega)$ may be determined by fitting the experimental $\zeta(\omega)$ to the form Eq. (6). Together, Eqs. (4) and (6) form a "generalized Saffman-Einstein" relation that can be used to analyze single-particle microrheology experiments.

Our initial motivation for deriving Eq. (6) was to analyze the data of [11]; we have applied this technique to extract the surface viscosity $\eta_m(\omega)$ from the mean-squared displacement data of [11] on the motion of membrane-anchored particles on freestanding dimyristoyl phosphatidylcholine (DMPC) bilayers. However, it has come to our attention that this experiment may be flawed [36]. To avoid any possible confusion, we do not include the analysis here as the extracted $\eta_m(\omega)$ is likely not physically meaningful. We do stress that the analysis of the data, as outlined in the preceding paragraph, was entirely straightforward, and application of our methods in the future to reliable experimental data should pose no difficulties.

In Ref. [11], the authors extract the correct drag $\zeta(\omega)$ from Eq. (4), but they interpret it with an effective three-dimensional complex shear modulus $G_{3\mathrm{D}}(\omega) = i\omega\zeta(\omega)/6\pi a$, motivated by the Stokes formula $\zeta = 6\pi\eta_m a$ for a spherical particle in a homogeneous medium. This does not distinguish between drag caused by the membrane and drag from the bulk fluid, and may be difficult to interpret [37].

We provide a simple example of the possible errors caused by assuming the Stokes drag is appropriate to the membrane geometry. We let the membrane be a simple Maxwell fluid, $\eta_m(\omega) = \eta_m(0)/(1 + i\omega\tau_c)$, and then calculate the drag $\zeta(\omega)$ from Eq. (6). We plot the effective $G_{3\mathrm{D}}(\omega) = i\omega\zeta(\omega)/6\pi a \equiv G'_{3\mathrm{D}}(\omega) + iG''_{3\mathrm{D}}(\omega)$ in Fig. 2. The actual shear modulus of the membrane, $G_{2\mathrm{D}}(\omega) = i\omega\eta_m(\omega)$, is plotted in the inset. The effective $G_{3\mathrm{D}}(\omega)$ does not necessarily reflect the underlying properties of the membrane, quantitatively or qualitatively.

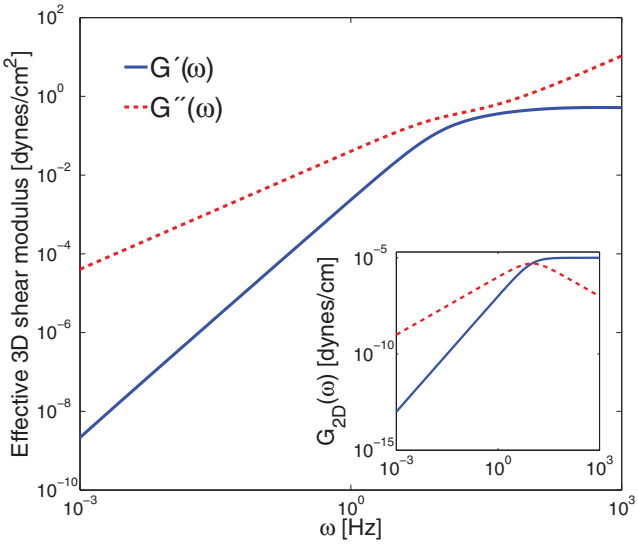

FIG. 2. (Color online) The effective three-dimensional shear modulus G_{3D} does not accurately represent the membrane's viscoelastic properties. We choose the underlying membrane surface viscosity $\eta_m(\omega)$ to have the Maxwell form, $\eta_m(0)/(1+i\omega\tau_c)$, with $\eta_m(0) = 10^{-6}$ poise cm and $\tau_c = 0.1$ s [$G_{2D} = i\omega\eta_m(\omega)$ is plotted in the inset]. $\rho_m = 5\times10^{-7}$ g/cm^2, $\rho_f = 1$ g/cm^3, and $a = 10^{-5}$ cm. The large-frequency behavior of $G_{3D}(\omega)$ is anomalously viscous, and the crossover time extracted from $G_{3D}(\omega)$ is also incorrect, $\tau_c \approx 0.043$ s.

Most strikingly, while we have assumed that the underlying membrane is elastic at frequencies larger than τ_c^{-1}, $G_{3D}(\omega)$ describes a system with a primarily viscous response at large frequencies (Fig. 2). This is a consequence of the bulk fluid; at large ω, $|\eta_m(\omega)|$ decreases as $1/\omega$, and the membrane surface viscosity becomes less relevant in comparison to the bulk fluid's viscosity. Thus, $G_{3D}(\omega)$ is only probing the bulk fluid at frequencies $\omega \gg \tau_c^{-1}$. This regime is not currently seen in the microrheology experiments of [11], which have a maximum observed frequency of roughly 30 Hz.

The competition between bulk and surface viscosity also affects the location of the crossover point. Normally, $G'(\omega) = G''(\omega)$ at $\omega_c = 1/\tau_c$, the crossover frequency. However, in Fig. 2, we see that G'_{3D} and G''_{3D} never cross; the location of closest approach is at $\omega \approx 23$ Hz, which corresponds to $\tau_c \approx 0.043$ s, less than half of the correct $\tau_c = 0.1$ s. This shows that using $G_{3D}(\omega)$ can induce systematic errors in quantitative measurements, even in frequency ranges where the qualitative picture is correct.

II. VISCOELASTICITY AND DOMAIN FLICKER SPECTROSCOPY

In earlier work, the authors and co-workers calculated the relaxation times of near-circular lipid domains in multicomponent membranes, and we used this to determine the surface viscosity of model membranes [16]. This earlier analysis only treated the case of a purely viscous membrane, but the extension to a viscoelastic membrane is fairly simple through applications of Eq. (3) and analogy the earlier viscous treatment. We can directly extract the complex surface viscosity by fitting experimentally measured autocorrelation

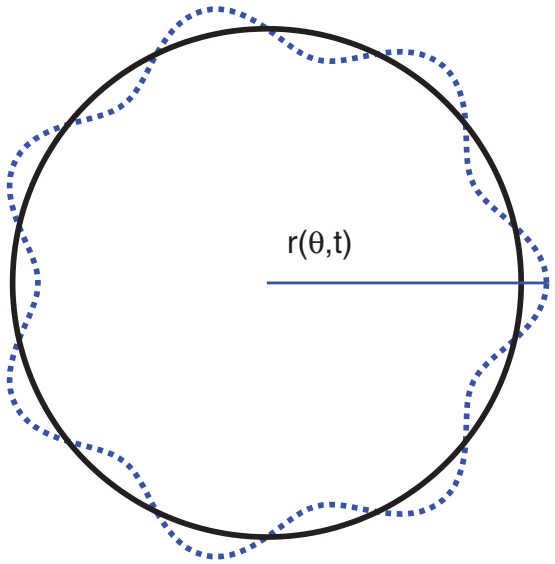

FIG. 3. (Color online) Illustration of quasicircular membrane domain. We describe the domain boundary as $r(\theta,t) = R[1+\frac{1}{2}\sum_{n\neq0} u_n(t)e^{in\theta}]$. For this figure, $r(\theta) = R(1+0.1\cos 7\theta)$, i.e., $u_7 = u_{-7} = 0.1$ (dashed line). The equilibrium shape is circular, $r(\theta,t) = R$ (solid line).

functions. We also present some exact results for Maxwell models.

As in [16], we describe the shape of a near-circular membrane domain by the Fourier series $r(\theta,t) = R[1+\frac{1}{2}\sum_{n\neq0} u_n(t)e^{in\theta}]$ (Fig. 3). If the domain is driven toward a circular shape by a line tension σ, and the membrane is purely viscous, the equations of motion for the membrane deformations u_n are

$$\frac{d}{dt}u_n = -u_n(t)/\tau_n + \xi_n(t), \tag{7}$$

where $\xi_n(t)$ is a Langevin force and the relaxation time τ_n is

$$\tau_n = \frac{\eta_m R}{\sigma}\frac{1}{n^2(n^2-1)}\left[\int_0^\infty dx \frac{J_n^2(x)}{x^2(x+\Lambda)}\right]^{-1}, \tag{8}$$

where $\Lambda = R/L_{SD}$, $L_{SD} = \eta_m/2\eta_f$. When the membrane is viscoelastic, the relaxation of the domain will be nonexponential, and depends on the history:

$$\frac{d}{dt}u_n(t) = -\int_{-\infty}^{+\infty} dt'\gamma_n(t-t')u_n(t') + \xi_n(t). \tag{9}$$

For causality, $\gamma_n(t) = 0$ for $t < 0$. The generalized Langevin equation of (9) is simpler in Fourier space:

$$u_n(\omega) = \frac{\xi_n(\omega)}{i\omega + \gamma_n(\omega)}. \tag{10}$$

The variance of the Langevin force $\xi_n(\omega)$ is set by the fluctuation-dissipation theorem [38],

$$\langle\xi_n(\omega)\xi_n^*(\omega')\rangle = 4\pi\langle|u_n|^2\rangle \mathrm{Re}\{\gamma_n(\omega)\}\delta(\omega-\omega'). \tag{11}$$

In the limit of linear viscoelastic flows where Eq. (3) applies, we can determine $\gamma_n(\omega)$ easily. In Ref. [16], we calculated τ_n by using the viscous membrane Oseen tensor Eq. (2) to determine the velocity of the fluid at the boundary

from the force caused by the deformation of the boundary. This derivation applies with minimal change to the generalized membrane Oseen tensor, yielding

$$\gamma_n(\omega) = \frac{\sigma n^2(n^2-1)}{R}\int_0^\infty dx \times \frac{J_n^2(x)}{x\left[i\omega\rho_m R^2 + x^2\eta_m(\omega) + 2\eta_f Rx\sqrt{1+\frac{i\omega\rho_f R^2}{\eta_f x^2}}\right]}. \quad (12)$$

We ignore inertia for the remainder of this section. The presence of the inertial term could lead to a long-time power-law tail in the correlation function (see Sec. III), but numerical computation of the autocorrelation $\langle u_n(t)u_n^*(0)\rangle$ using Eq. (12) suggests that it would become important only when the correlation function reached $\sim 10^{-6}$ of its initial value; this is effectively unobservable. Instead, we use the noninertial approximation,

$$\gamma_n(\omega) = \frac{\sigma n^2(n^2-1)}{R}\int_0^\infty dx \frac{J_n^2(x)}{x^2[x\eta_m(\omega) + 2\eta_f R]}. \quad (13)$$

A. Extraction of the frequency-dependent surface viscosity

The fluctuation-dissipation relationship for our generalized Langevin equation can be written [38]

$$\frac{1}{i\omega + \gamma_n(\omega)} = \frac{1}{\langle |u_n|^2\rangle}\int_0^\infty dt\, e^{-i\omega t}\langle u_n^*(t_0)u_n(t_0+t)\rangle. \quad (14)$$

If we define $C_n(\omega) = \int_0^\infty dt\, e^{-i\omega t}\langle u_n^*(t_0)u_n(t_0+t)\rangle/\langle |u_n|^2\rangle$, then we can determine $\gamma_n(\omega) = 1/C_n(\omega) - i\omega$. In practice, using the Laplace transform version of this relation is simpler, as the long-time behavior of the correlation function is unreliable due to statistical fluctuations. The Laplace transform of the correlation function, $\hat{C}_n(s) \equiv \int_0^\infty dt\, e^{-st}\langle u_n^*(t_0)u_n(t_0+t)\rangle/\langle |u_n|^2\rangle$, takes on the form

$$\hat{C}_n(s) = \frac{1}{s + \hat{\gamma}_n(s)}, \quad (15)$$

where

$$\hat{\gamma}_n(s) = \frac{\sigma n^2(n^2-1)}{R}\int_0^\infty dx \frac{J_n^2(x)}{x^2[x\eta_m(s) + 2\eta_f R]}. \quad (16)$$

To analyze a trace of a fluctuating domain, $r(\theta,t)$, we first expand $r(\theta,t)$ into Fourier modes, $r(\theta,t) = R[1 + \frac{1}{2}\sum_{n\neq 0} u_n(t)e^{in\theta}]$. The line tension σ is determined from $\langle |u_n|^2\rangle$ as in [16]. We then calculate the Laplace transform of the autocorrelation of u_n, $\hat{C}_n(s)$. We fit $\hat{\gamma}_n^{\rm exp}(s) \equiv 1/\hat{C}_n(s) - s$ to Eq. (16). We do this by, for each frequency s, determining the viscosity $\eta_m(s)$ that makes Eq. (16) the best fit to $\hat{\gamma}_n^{\rm exp}(s)$ for all observed modes n simultaneously. This is a generalization of the analysis of [16], in which $\eta_m(0)$ was determined by fitting the relaxation times τ_n as a function of n.

We apply this procedure to experimental data on domains in diphytanoylphosphatidylcholine/Cholesterol/dipalmitoylphosphatidylcholine (DiPhyPC/Chol./DPPC) vesicles from [16]. Because of the limited spatial resolution of domain flicker spectroscopy experiments [15], we only fit over modes $n = 2$–5. Typical results for $\eta_m(s)$ are shown in Fig. 4. The data show a possible viscoelastic dependence of the surface viscosity η_m on frequency, which can be roughly fitted by a Maxwell model, $\eta_m(s) = \eta_m(0)/(1 + s\tau_c)$. For a purely viscous membrane, $\eta_m(s)$ would be constant. The mean crossover time τ_c measured is $\tau_c = 7.3 \pm 2$ ms; this differs from the crossover time of $\approx$100 ms reported in Harland *et al.* [11]; see, however, Ref. [36] and our earlier comments.

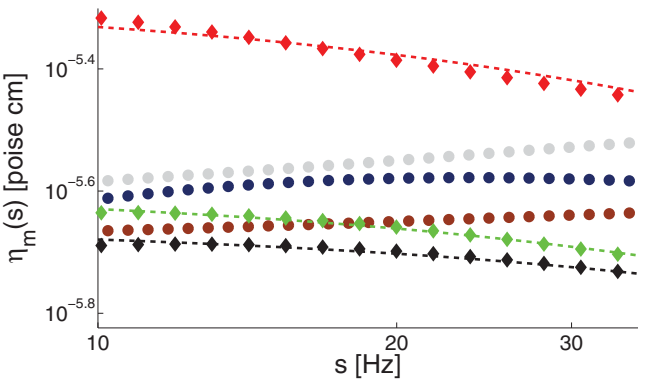

FIG. 4. (Color online) Typical $\eta_m(s)$ extracted from experimental data (diamonds) and simulations assuming a purely viscous membrane (circles). Fits to the Maxwell model are shown for experimental data, with crossover times of 18, 8.2, and 5.0 ms (from top to bottom). Simulation points do not show significant decreases at large s, which are present in the experimental points. All simulation traces assume a domain in a purely viscous membrane with $\eta_m = 3 \times 10^{-6}$ poise cm, $\sigma = 0.15$ pN, $R = 4$ μm, tracked for 6 s $= 15\tau_2$. This is comparable to the experimental domains shown, which have radii of roughly 4 μm, line tensions $\sigma = 0.1$–0.25 pN, and $\eta_m(0) \approx (2$–$6) \times 10^{-6}$ poise cm (determined by fit), and are tracked for roughly 5 s. The bulk viscosity of water, $\eta_f = 0.01$ poise, is assumed in both cases.

Because of the complicated analysis procedure, and the potential relevance of statistical fluctuations, we also apply our fitting procedure to a simulated trace $r(\theta,t)$ constructed assuming that the membrane is purely viscous, i.e., $u_n(t)$ is an Ornstein-Uhlenbeck process [39] simply given by Eq. (7). We see that statistical fluctuations alone cannot explain the observed dependence of $\eta_m(s)$ on s; the simulated data do not show any tendency toward a significant decrease in $\eta_m(s)$ with s (Fig. 4).

We note, however, that the range of frequencies covered by this analysis is small, and that the relaxation time determined is near the shortest such time that could be observed in this analysis. The frequency range displayed in Fig. 4 is limited by the camera acquisition rate and the statistical fluctuations in the autocorrelation function. Current experiments [15,16] only track domain flickering over a period of roughly 10–100 correlation times. In Fig. 5, we show typical statistical fluctuations in the autocorrelation function, both from experiment and assuming only a simple exponential decay [$u_n(t)$ is an Ornstein-Uhlenbeck process as above]. Clearly, the autocorrelation function is only reliable over the first few correlation times. This sets the lower bound for our frequency range, at $s_{\rm min} \approx 1/\tau_n$. The upper bound is set by the Nyquist frequency, $s_{\rm max} = 1/2\Delta t$, where Δt is the acquisition time (15 ms in [16]). For the experimental data from [16], the accessible frequency range is roughly 10–30 Hz. An improved

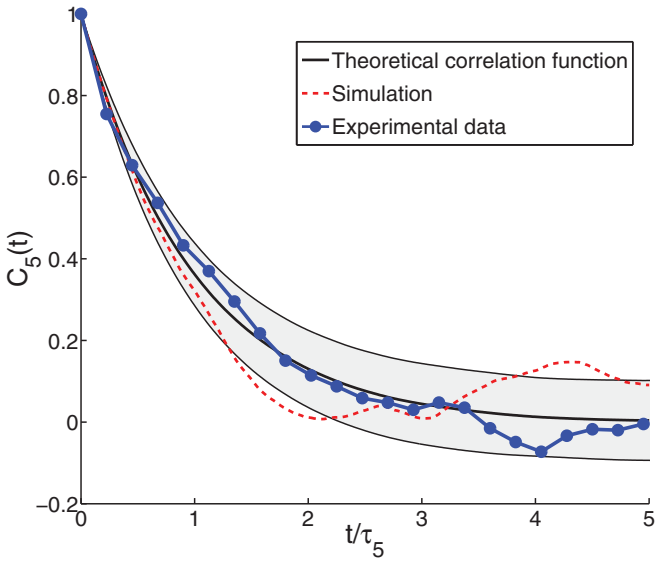

FIG. 5. (Color online) The autocorrelation function $C_n(t) = \langle u_n(t)u_n^*(0)\rangle/\langle|u_n|^2\rangle$ calculated from a trajectory of finite time has statistical fluctuations from its theoretical value (solid line). The gray area indicates the one-standard-deviation uncertainty in $C_n(t)$, and the dashed line is from a particular realization of $C_n(t)$. To calculate these, we have assumed that the purely viscous equation of motion Eq. (7) holds, and we have evaluated a trajectory of 100 correlation times. Experimental data from [16] shows similar fluctuations for a similar trajectory length; the domain trace shown is $n = 5$ for a domain with $\sigma = 0.12$ pN and $R = 3.1$ μm, tracked for 4.8 s, or 72 correlation times for the $n = 5$ mode.

range of frequencies may be reached if domains are observed over a longer time, or with better temporal resolution.

Though the procedure we have outlined here is model-independent, it is interesting to treat the special case of a membrane described by a Maxwell model, which the data of [16] and Harland *et al.* [11] generally support [36]. We can develop some exact results for the autocorrelation function $C_n(t)$ for a Maxwell model (Appendix D). We see that the domain autocorrelation function $C_n(t)$ in Maxwell viscoelastic systems is typically biexponential. The short-time behavior is set by the bulk fluid, as the surface viscosity $\eta_m(\omega)$ is small at high frequencies. At long times, an anomalously slow long-time decay of large-n and high-σ modes is observed, with a decay constant set by the viscoelastic crossover time τ_c. Therefore, if the membrane is viscoelastic with a time scale τ_c on the order of τ_n, we would observe systematic deviations from Eq. (8); large-n modes would have slower decays than predicted by the purely viscous theory. No such systematic deviations are observed (see the supplementary material of [16]), suggesting that τ_c is smaller than the shortest decay times measured there, which are of order 10 ms. This is consistent with our above analysis (Fig. 4), which found $\tau_c \approx 7$ ms.

III. LONG-TIME TAILS IN A MEMBRANE

Our generalized membrane Oseen tensor, Eq. (3), suggests that inertial effects of the outside fluid should only become appreciable for $\omega \sim \omega_f(k)$, i.e., for flows when the unitless number $\rho_f L_c^2/\eta_f T_c$ is non-negligible, where L_c is a characteristic length scale and T_c is a characteristic time. However, even at long times, fluid inertia can have an effect on the diffusion of particles within a fluid. A naive Langevin approach predicts that the velocity autocorrelation correlation function for a tagged particle $C_{vv}(t) \equiv \langle \mathbf{v}_p(t_0 + t) \cdot \mathbf{v}_p(t_0)\rangle$ decays exponentially at long times [40]. However, molecular-dynamics simulations [41] and experiments [42] observe power-law autocorrelations at long times, with $C_{vv}(t) \sim t^{-1}$ in two dimensions and $C_{vv}(t) \sim t^{-3/2}$ in three dimensions. These "long-time tails" have been shown theoretically to be a consequence of the inertia of the fluid surrounding the particle [43–45].

Viscous membranes are often referred to as "quasi-two-dimensional fluids" in that their response function $T^{ij}(r)$ [Eq. (2)] changes from a two-dimensional behavior $T \sim \ln(r)$ for $r \ll L_{\mathrm{SD}}$ to a three-dimensional one, $T \sim 1/r$ at $r \gg L_{\mathrm{SD}}$, where L_{SD} is the Saffman-Delbrück length [5]. Two- and three-dimensional fluids also have different long-time tails. In two dimensions, $C_{vv}(t) \sim t^{-1}$ and the diffusion coefficient $D = \frac{1}{d}\int_0^\infty dt\, C_{vv}(t)$ diverges logarithmically; this is related to Stokes' paradox, in which the diffusion constant of a circle in a two-dimensional creeping flow diverges [46]. In membranes, the divergence of the diffusion coefficient is regulated by the presence of the bulk fluid [1], so $C_{vv}(t) \sim t^{-\alpha}$ with $\alpha > 1$. We can use the tools developed above to calculate α through simple mode-coupling theory. We will first treat the case of a purely viscous membrane, $\eta_m(\omega) = \eta_m(0)$.

Applying mode-coupling theory lets us calculate the velocity autocorrelation function of a tagged lipid as in the pure two- or three-dimensional case [43,47],

$$C_{vv}(t) = C_{vv}^{\mathrm{fast}}(t) + \frac{1}{\mathcal{L}^4}\sum_{\mathbf{k}} e^{-Dk^2 t}\langle \mathbf{v}_m(\mathbf{k},t_0 + t) \cdot \mathbf{v}_m^*(\mathbf{k},t_0)\rangle, \tag{17}$$

where D is the bare self-diffusion coefficient (lipid diffusion coefficient in our case) and $\mathcal{L}$ is the system's linear size. We can calculate the autocorrelation function of $\mathbf{v}_m(\mathbf{k})$ from Eq. (A19). We move to Laplace transform space, $\hat{f}(s) \equiv \int_0^\infty dt\, e^{-st} f(t)$, finding (with no external forces)

$$\hat{\mathbf{v}}_m(\mathbf{k},s) = \frac{\rho_m \mathbf{v}_m(\mathbf{k},t = 0)}{\rho_m s + k^2\eta_m + 2k\eta_f\sqrt{1 + s/\omega_f(k)}}, \tag{18}$$

which allows us to write, using the usual inverse Laplace transform,

$$\langle \mathbf{v}_m(\mathbf{k},t_0 + t) \cdot \mathbf{v}_m^*(\mathbf{k},t_0)\rangle = \int_{\delta - i\infty}^{\delta + i\infty} \frac{ds}{2\pi i}\, e^{st}\, \frac{\rho_m\langle|\mathbf{v}_m(\mathbf{k})|^2\rangle}{\rho_m s + k^2\eta_m + 2k\eta_f\sqrt{1 + s/\omega_f(k)}}. \tag{19}$$

The variance $\langle|\mathbf{v}_m(\mathbf{k})|^2\rangle$ is set by equipartition, noting we only have one independent component because of the incompressibility constraint $\mathbf{k} \cdot \mathbf{v}_m(\mathbf{k}) = \mathbf{0}$,

$$\langle|\mathbf{v}_m(\mathbf{k})|^2\rangle = k_B T\mathcal{L}^2/\rho_m. \tag{20}$$

We can use the tools of complex analysis to reduce Eq. (19) to a more manageable form by deforming the contour so that the integral is taken along the branch cut of the square-root function. [Up to a variable substitution, $s \to s + \omega_f(k)$, this

process follows a similar calculation for the three-dimensional case given in [48].] The result is ($t > 0$)

$$\langle \mathbf{v}_m(\mathbf{k},t_0+t)\cdot\mathbf{v}_m^*(\mathbf{k},t_0)\rangle = \int_0^\infty \frac{dx}{\pi}\, e^{-(x+\omega_f)t}\, \frac{2k_BT\mathcal{L}^2k\eta_f\sqrt{x/\omega_f}}{(\eta_m k^2-\rho_m\omega_f-\rho_m x)^2+(2k\eta_f)^2 x/\omega_f}. \tag{21}$$

We will eventually wish to evaluate this integral in the limit $t\to\infty$, and so this equation will be dominated by small x, $x \ll 1/t$. The leading term in x as $x\to 0$ in the integrand is of order $\sqrt{x}$; however, large-k modes are also suppressed at long times by the term $e^{-\omega_f(k)t} = e^{-\eta_f k^2 t/\rho_f}$, and the naive expansion in x fails. We expect $x \sim k^2 \sim 1/t$, and so to the leading order in $1/t$,

$$\langle \mathbf{v}_m(\mathbf{k},t_0+t)\cdot\mathbf{v}_m^*(\mathbf{k},t_0)\rangle = \frac{k_BT}{2\pi}\mathcal{L}^2 e^{-\omega_f(k)t}\int_0^\infty dx\, \frac{e^{-xt}}{\sqrt{\rho_f\eta_f x}} \tag{22}$$

$$= \frac{k_BT}{2\pi}\mathcal{L}^2 e^{-\omega_f(k)t}\sqrt{\frac{\pi}{\rho_f\eta_f t}}. \tag{23}$$

Inserting this result into Eq. (17) and assuming a large system, $\mathcal{L}^{-2}\sum_k \to \int \frac{d^2k}{(2\pi)^2}$, we find

$$C_{vv}^{\rm slow}(t) \sim \frac{k_BT}{4\pi}\sqrt{\frac{1}{\pi\rho_f\eta_f t}}\int_0^\infty dk\, k e^{-(D+\eta_f/\rho_f)k^2 t} \tag{24}$$

$$\sim \frac{k_BT}{8\pi}\sqrt{\frac{1}{\pi\rho_f\eta_f}}\frac{1}{D+\eta_f/\rho_f}t^{-3/2}. \tag{25}$$

Thus, self-diffusion in membranes should show the usual three-dimensional long-time tails of $t^{-3/2}$. Note that in taking the small-k, long-length limit, we have eliminated all dependence of the velocity autocorrelation function on the membrane parameters, as would be expected. For comparison, in a pure d-dimensional fluid [43],

$$C_{vv}^{\rm slow}(t) \sim (d-1)\frac{k_BT}{\rho}\left[4\pi(D+\eta/\rho)t\right]^{-d/2} \quad \text{(pure fluid)}. \tag{26}$$

Our asymptotic result for the long-time tail in a membrane, Eq. (25), has the time dependence of a three-dimensional system, but depends on the combination $(D+\eta/\rho)$ as in a two-dimensional fluid. (In the limit of $\eta_f/\rho_f \gg D$, our result reduces exactly to the three-dimensional fluid result.)

In the asymptotic limit $t\to\infty$, the velocity correlation function is independent of the membrane viscosity and density. Can we observe the presence of the membrane at shorter times? Numerically evaluating $C_{vv}^{\rm slow}(t)$ using Eq. (17) with Eq. (21) [assuming $\mathcal{L}^{-2}\sum_k \to (2\pi)^{-2}\int d^2k$] shows that $C_{vv}^{\rm slow}(t)$ crosses over between pure two-dimensional behavior, Eq. (26), and the quasi-2D tail Eq. (25) (Fig. 6). We can understand the crossover simply in terms of a simple heuristic argument [47]. The linearized Navier-Stokes equations describe diffusion of vorticity, with diffusion coefficient $\nu = \eta/\rho$; if a tagged particle has an initial velocity $\mathbf{V}_p(0)$, after a time t, this velocity will be spread out over a region of space of volume $V_t = (\nu t)^{d/2}$, and shared among nV_t particles, where n is the number density. Thus we expect $C_{vv}(t) \sim 1/nV_t$, which reproduces the classical $t^{-d/2}$ tail Eq. (26). In the case of a membrane, momentum is transported both directly through the membrane, with kinematic viscosity $\nu_m = \eta_m/\rho_m$, and through the fluid, with kinematic viscosity $\nu_f = \eta_f/\rho_f$. Thus we expect $C_{vv}^{\rm mem}(t) \sim 1/\rho_m\nu_m t$ and $C_{vv}^{\rm bulk} \sim 1/\rho_f\left(\nu_f t\right)^{3/2}$. Comparing these two results, we see that the crossover between membrane-dominated long-time tails and bulk fluid-dominated long-time tails should occur at $t \sim t_* \equiv \rho_f\eta_m^2/\eta_f^3$. This predicts a crossover at $\sim 10^{-6}$ s for the parameters of Fig. 6, consistent with our results. Changing the parameters η_m, η_f, and ρ_f and then numerically evaluating the mode-coupling result confirms this result. Most notably, changing the bulk fluid viscosity by a factor of 10 will change the crossover time by three orders of magnitude.

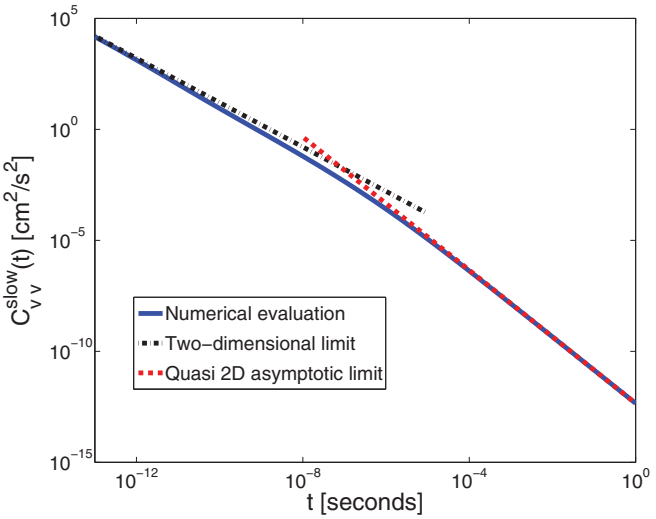

FIG. 6. (Color online) Velocity autocorrelation function $C_{vv}^{\rm slow}(t)$, evaluated numerically from the mode-coupling theory for a purely viscous membrane, Eqs. (17) and (21) (solid line). Crossover between the two-dimensional behavior, Eq. (26) ($d = 2$), and the full quasi-2D limit, Eq. (25), is observed. Parameters chosen here are $\eta_m = 10^{-6}$ poise cm, $\eta_f = 0.01$ poise, $\rho_m = 5\times 10^{-7}$ g/cm^2, $\rho_f = 1$ g/cm^3, $D = 10^{-9}$ cm^2/s, and $T = 21\,^\circ$C.

These long-time tails may be observable in hydrodynamic simulations in the membrane geometry, e.g., [49], although there are well-known difficulties in the simulation of long-time tails [50]. An additional concern is that the crossover between two- and three-dimensional tails may be difficult to observe; in some dissipative particle dynamics simulations of membranes, such as [49], the membrane viscosity is of the order of the fluid viscosity, which would significantly decrease the crossover time to roughly 10^{-10} s.

The $t^{-3/2}$ tail is not only present in the diffusion of a point particle, it also applies to the diffusion of an extended embedded object in a membrane, at least if the immersed-boundary approximation is assumed (see Appendix B). This raises the possibility of observing these tails in the velocity autocorrelation functions of colloids at interfaces, as in the experiments of Prasad, Koehler, and Weeks [7].

Figure 6 shows the long-time tails for a purely viscous membrane. In three-dimensional fluids, the long-time tails may be strongly affected by the viscoelastic properties of the

fluid [51]. For membranes, however, the asymptotic long-time tail reflects the properties of the bulk fluid surrounding the membrane, and so as long as the membrane is viscous at long times [$\eta_m(0)$ is finite], viscoelastic membranes will also have a $t^{-3/2}$ tail. However, the intermediate region may be quite different from that shown in Fig. 6. Zwanzig and Bixon [43] note that a simple Maxwell model of viscoelasticity in a three-dimensional fluid leads to anticorrelations in the velocity autocorrelation function. This behavior is also seen in membranes, although the presence of the outside fluid presents an added complication. Consider a membrane-embedded object with radius a oscillating at a frequency ω: we expect that if $a \gg |\eta_m(\omega)|/2\eta_f = L_{\mathrm{SD}}(\omega)$, the primary source of drag will be the outside fluid, which is purely viscous. This effect is not well-captured by the mode-coupling theory, which only treats a point particle. To determine the behavior of the velocity autocorrelation function, we evaluate

$$C_{vv}(t) = k_B T \int_{-\infty}^{\infty} \frac{d\omega}{\pi} e^{i\omega t} \mathrm{Re} \frac{1}{i\omega M + \zeta(\omega)}, \qquad (27)$$

where $\zeta(\omega)$ is given by the immersed-boundary approximation, Eq. (6).

We assume a Maxwell model, $\eta_m(\omega) = \eta_m(0)/(1 + i\omega\tau_c)$, and numerically evaluate Eq. (27) using the fast Fourier transform. $C_{vv}(t)/C_{vv}(0)$ is plotted for two systems in Figs. 7 and 8. We notice several basic features of these curves. Initial exponential decay is observed, as we would expect from the high-frequency asymptotic limit of Eq. (27), and a crossover into anticorrelation is seen. If a or τ_c is large, this anticorrelation may not be immediately evident (Fig. 7). The autocorrelation function becomes positive again for $t \gg \tau_c$, and the asymptotic long-time tail is once again $t^{-3/2}$.

For smaller objects and shorter τ_c, a dip in the autocorrelation function may be immediately apparent (Fig. 8). Wohlert and Edholm observe velocity anticorrelations in atomistic simulations of DMPC up to times of 10 ps [52], suggesting that τ_c for this system is at least 10 ps. This is not terribly

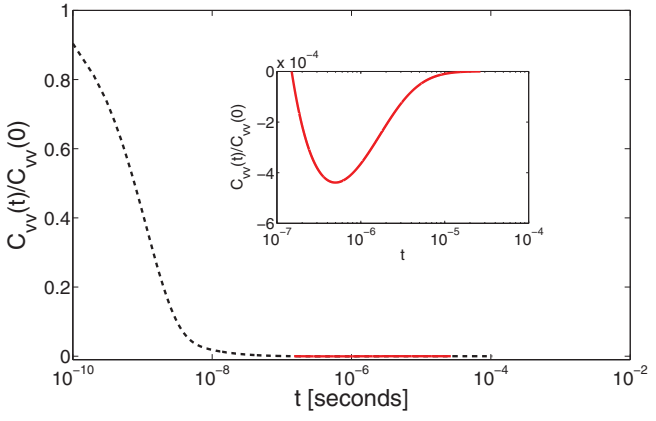

FIG. 7. (Color online) Velocity autocorrelation function $C_{vv}(t)/C_{vv}(0)$, evaluated numerically from Eq. (27). Parameters chosen here are $\eta_f = 0.01$ poise, $\rho_m = 5 \times 10^{-7}$ g/cm^2, $\rho_f = 1$ g/cm^3, $a = 10^{-5}$ cm, and $M = 10^{-14}$ g. The surface viscosity is $\eta_m(\omega) = \eta_m(0)/(1 + i\omega\tau_c)$ with $\eta_m(0) = 10^{-6}$ poise cm and $\tau_c = 10^{-5}$ s. The solid portion indicates where C_{vv} is negative; this region is replotted in the inset.

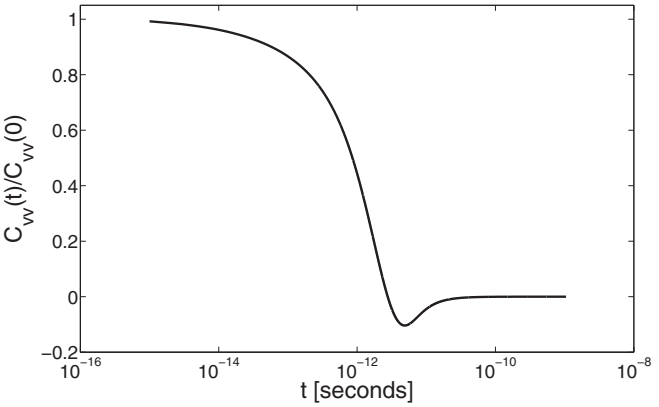

FIG. 8. (Color online) Velocity autocorrelation function $C_{vv}(t)/C_{vv}(0)$, evaluated numerically from Eq. (27) for a smaller, lipid-scale immersed particle. Parameters chosen here are the same as Fig. 7, except with $a = 10^{-9}$ cm, $M = 10^{-21}$ g, and the crossover time $\tau_c = 10^{-9}$ s. A clear anticorrelation is observed for times smaller than τ_c.

surprising, given measurements of τ_c that are no smaller than microseconds [13]. The crossover to a positive autocorrelation function is not observed in [52], making it difficult to determine a realistic estimate for the crossover time τ_c.

We also note that $C_{vv}(0)$, as determined by Eq. (27), is not necessarily equal to $\langle |\mathbf{V}_p|^2 \rangle_{\mathrm{bare}} = k_B T/M$. If $\zeta(\omega) \to i\omega m$ at large ω, the mass M will be renormalized, and $C_{vv}(0) = k_B T/(M + m)$. This is well known for the simple three-dimensional pure fluid case [48], where the additional mass m is roughly the mass of fluid displaced by the particle.

The long-time tails in a membrane were previously calculated by Seki and Komura [53], who found exponential decay, and Serra and Rubí [28], who found a t^{-1} tail. Seki and Komura assume a phenomenological momentum loss in place of the outside fluid; this assumption leads to the loss of the long-time tails. The simple linear drag used is, however, appropriate for the case of supported membranes in certain limits [54]. Serra and Rubí use the correct hydrodynamics for a free membrane surrounded by an external fluid, but they only evaluate the long-time tails in the limit of weak coupling with the outside membrane. Our results show that this is not the asymptotic result, but may be observed for times $t < t_* = \rho_f \eta_m^2/\eta_f^3$.

IV. DISCUSSION

We have developed a generalization of the usual membrane Oseen tensor to include the inertia of both the membrane fluid and the bulk fluid surrounding it, as well as the viscoelasticity of the membrane. We applied this membrane Oseen tensor to three problems of dynamics in a membrane. First, we wrote down a simple mobility that allows us to analyze single-particle microrheology experiments in a membrane using a "Saffman-Einstein" relationship. We demonstrated that naively applying the 3D Stokes-Einstein formula will cause both qualitative and quantitative errors in determining the viscoelastic properties of a membrane. Second, we showed how domain flicker spectroscopy can be used to extract linear viscoelastic properties of the membrane; we observed viscoelastic behavior with time constants $\tau_c < 10$ ms. We

also derived some exact results for membranes with simple Maxwell viscoelastic behavior, showing that relaxation is typically bi-exponential, with a long-time behavior that is anomalously slow compared to the simple viscous theory. Third, we analyzed the behavior of velocity autocorrelation functions within a membrane, and demonstrated that quasi-two-dimensional fluids have $t^{-3/2}$ tails asymptotically, but for times small compared with the 2D-3D crossover time $t_* \sim \rho_f \eta_m^2/\eta_f^3$, the two-dimensional t^{-1} tail may be observed for a purely viscous membrane. For a viscoelastic membrane, anticorrelations may be present at short times.

The viscoelastic crossover time measured here, $\tau_c \approx 7$ ms, warrants some discussion. It disagrees with earlier measurements on pure lipid bilayers that found crossover times of 37 μs [13]. However, those measurements were performed on membranes of glycerol mono-oleate rather than multicomponent mixtures with cholesterol. Because the membranes we study are not homogeneous, the membrane will be viscoelastic on length scales much larger than the membrane domain size, with relaxation times comparable to domain relaxation times, i.e., 0.1–1 s; this is in direct analogy to the viscoelasticity of an emulsion composed of Newtonian fluids [55]. We are probing the dynamics on scales of R_{domain}/n, where n is the mode studied, and so we do not believe we are observing this long-scale effective-medium response. The multicomponent membranes analyzed here and in [16] exhibit a coexistence between liquid disordered and liquid ordered phases [56]; the ordered phase is known to have smaller lipid diffusion coefficients than the disordered phase [57], and has a higher bending modulus [58]. It is plausible that the liquid ordered phase has an elastic response, as the gel phase does [14], though a recent experiment did not observe this response in liquid-ordered monolayers [59]. Our analysis assumes that the domain and the surrounding membrane have the same complex surface viscosity $\eta_m(\omega)$. The authors and co-workers have suggested that domain flicker spectroscopy can be interpreted in terms of a single "effective viscosity," which is the average of the domain and surrounding membrane viscosity [16], and this may also be the case for viscoelastic membranes. The effective viscosity picture will clearly be true in the limit $R_{\text{domain}}/n \ll L_{\text{SD}}$, where the dissipation from the membrane is more relevant than that from the bulk fluid, as can be seen from applying the viscous-viscoelastic correspondence to the result of Mann *et al.* [60].

We also expect that the generalized membrane Oseen tensor we present here will be useful in a variety of applications beyond what we have developed in this paper. In the phase separation of two-dimensional binary fluids, dynamical scaling occurs when the force from line tension is balanced against fluid inertia [61–63]; the presence of dynamical scaling in membranes is controversial, and has recently been discussed by our group and others [6,64] using the membrane Oseen tensor. Our result may also be useful for analyzing molecular-dynamics simulations of membranes that explicitly include inertia [49]. The full frequency-dependent Oseen tensor may also be relevant in calculations of the renormalization of viscosities near the critical point [65].

Throughout this paper, we have assumed that the basic Saffman-Delbrück quasi-two-dimensional fluid model is valid. In particular, we assume Eq. (6) is appropriate for microrheological measurements on membranes. Proteins [66] as well as micron-scale lipid domains [3,4] have been observed to have diffusion coefficients consistent with the Saffman-Delbrück model, though there is some controversy on this point for membrane proteins [67]. Coupling between embedded objects and the deformation of the membrane can also in principle alter the diffusive behavior of the embedded particle [68,69]. Experimental applications of Eq. (6) should be paired with confirmation that the Saffman-Delbrück model is appropriate, either by variation of the probe size, a, or by studying the two-particle microrheological response as in [7]. As in the three-dimensional case, two-dimensional microrheological experiments should be less sensitive to local changes in the material induced by the probe particles [70].

We have also assumed that the membrane is surrounded by a purely viscous fluid; if the bulk fluid is also viscoelastic, our generalized Oseen tensor, Eq. (3), holds with a complex $\eta_f(\omega)$, as noted by Granek [71].

ACKNOWLEDGMENTS

We would like to thank Tobias Baumgart and Cinzia Esposito for the use of their data on domain flickering. This work was supported in part by the NSF (Grant Nos. CHE-0848809 and CHE-032168) and the BSF (Grant No. 2006285). B.A.C. acknowledges the support of the Fannie and John Hertz Foundation. F.L.H.B. acknowledges the Camille Dreyfus Teacher-Scholar Awards Program.

APPENDIX A: RESPONSE FUNCTION OF A VISCOELASTIC MEMBRANE INCLUDING INERTIA

We briefly review the application of the viscous-viscoelastic correspondence to a membrane below; our development follows that of [19].

The usual linearized Navier-Stokes equation ("unsteady Stokes equation") for an incompressible fluid can be written

$$\rho \frac{\partial \mathbf{v}(\mathbf{r},t)}{\partial t} = \nabla \cdot \overleftrightarrow{\tau} - \nabla P + \mathbf{f} \tag{A1}$$

$$\nabla \cdot \mathbf{v} = \mathbf{0}, \tag{A2}$$

where $\mathbf{f}$ is an applied force, and for a Newtonian fluid, the tensor $\overleftrightarrow{\tau}$ is given by $\overleftrightarrow{\tau} = 2\eta \overleftrightarrow{D}$, where η is the fluid viscosity and

$$\overleftrightarrow{D} = \tfrac{1}{2}[\nabla \mathbf{v} + (\nabla \mathbf{v})^T] \tag{A3}$$

is the rate-of-strain tensor. This gives us the usual form of the unsteady Stokes equation,

$$\rho \frac{\partial \mathbf{v}(\mathbf{r},t)}{\partial t} = \eta \nabla^2 \mathbf{v} - \nabla P + \mathbf{f} \tag{A4}$$

The constitutive relationship between $\overleftrightarrow{\tau}$ and $\overleftrightarrow{D}$ is more complicated for a viscoelastic fluid, as the stress can depend on the strain-rate history. We only treat linear viscoelastic fluids [19,20,72], where the stress varies linearly with strain rate as

$$\overleftrightarrow{\tau}(t) = 2 \int_{-\infty}^{\infty} dt' \, \eta(t - t')' \overleftrightarrow{D}(t'), \tag{A5}$$

where, for causality, $\eta(t) = 0$ for $t < 0$. In Fourier space, the convolution Eq. (A5) becomes a simple product,

$$\overleftrightarrow{\tau}(\omega) = 2\eta(\omega)\overleftrightarrow{D}(\omega), \tag{A6}$$

where $\eta(\omega) = \int_{-\infty}^{\infty} dt\, \eta(t) e^{-i\omega t}$. We note that in this framework, a purely viscous fluid corresponds to $\eta(\omega) = \eta(0) =$ const, or $\eta(t) = \eta(0)\delta(t)$. Substituting in this result to the Fourier transform of the Navier-Stokes equation gives us the viscoelastic unsteady Stokes equations

$$i\omega\rho\mathbf{v}(\mathbf{r},\omega) = \eta(\omega)\nabla^2\mathbf{v}(\mathbf{r},\omega) - \nabla P(\mathbf{r},\omega) \tag{A7}$$

This is precisely the Fourier transform of the usual linearized Navier-Stokes equation (A4), but with a complex viscosity $\eta(\omega)$. This shows that solutions to the unsteady Stokes problem for a viscous fluid can be directly transformed into solutions for the viscoelastic problem by changing the viscosity to a complex, frequency-dependent viscosity $\eta(\omega)$. This includes the response function to a point force (commonly referred to as the Oseen tensor).

If we describe a membrane as a two-dimensional incompressible viscoelastic fluid, coupled to a viscous bulk fluid [1,5,17,18], we have the equations of motion for the membrane velocity $\mathbf{v}_m$,

$$i\omega\rho_m\mathbf{v}_m(\mathbf{r},\omega) = \eta_m(\omega)\nabla^2\mathbf{v}_m - \nabla P_m + 2\eta_f\partial_z\mathbf{v}_f|_{z=0} + \mathbf{f}, \tag{A8}$$

$$\nabla\cdot\mathbf{v}_m = \mathbf{0}, \tag{A9}$$

where ρ_m is the membrane mass density and η_m is its surface viscosity. Note that these are two-dimensional quantities; the units of ρ_m are grams per square centimeter, and η_m is measured in poise cm (surface poise, or g/s). $\mathbf{f}$ is an applied force, $\mathbf{r} = (x,y)$ is the planar separation. We will indicate functions that have z dependence explicitly. $\mathbf{v}_f$ is the velocity of the three-dimensional fluid, which has equations of motion

$$i\omega\rho_f\mathbf{v}_f(\mathbf{r},z,\omega) = \eta_f\nabla^2\mathbf{v}_f - \nabla P_f \tag{A10}$$

$$\nabla\cdot\mathbf{v}_f = \mathbf{0}. \tag{A11}$$

The boundary conditions require that the velocity is continuous at the membrane at all times, $\mathbf{v}_f(\mathbf{r},z=0,t) = \mathbf{v}_m(\mathbf{r},t)$, and that the bulk fluid is at rest far from the membrane, $\mathbf{v}_f(\mathbf{r},z) \to 0$ as $|z| \to \infty$.

In the limit of creeping flow, where the inertial term in Eq. (A10) is discarded, the bulk fluid velocity $\mathbf{v}_f$ can be simply expressed in terms of the membrane velocity $\mathbf{v}_m$, allowing the dependence on $\mathbf{v}_f$ to be eliminated from Eq. (A8) [17]. If we retain the inertial term, then $\mathbf{v}_f$ is a true dynamic variable, and eliminating it will cause the Markovian system of Eqs. (A8)–(A11) to become history-dependent, even in the limit of a purely viscous fluid.

We can use linearity to determine the membrane's response function by treating single modes, as in [18]. Suppose that the membrane velocity is a simple transverse shear mode,

$$\mathbf{v}_m(\mathbf{r},t) = V_o\hat{\mathbf{y}}\, e^{i(kx+\omega t)}. \tag{A12}$$

We have chosen the shear mode to travel in the x direction without loss of generality, and the mode must be transverse to satisfy $\nabla\cdot\mathbf{v}_m = \mathbf{0}$. We then make the ansatz that the bulk fluid velocity is simply proportional to the fluid velocity; this guess is motivated by exact solutions to the coupled equations of motion (e.g., [2,9]). Then for $z > 0$, $\mathbf{v}_f$ is given by

$$\mathbf{v}_f(\mathbf{r},z,t) = V_o\hat{\mathbf{y}}\, f(z)\, e^{i(kx+\omega t)}. \tag{A13}$$

The boundary conditions on $\mathbf{v}_f$ require that $f(0) = 1$ and $f(z) \to 0$ as $z \to \infty$. Taking the curl of Eq. (A10) yields the equation

$$i\omega\rho_f f(z) = \eta_f\left(\frac{d^2 f}{dz^2} - k^2 f\right). \tag{A14}$$

The only solution to this equation that satisfies the boundary conditions is

$$f(z) = \exp[-kz\sqrt{1 + i\omega/\omega_f(k)}], \tag{A15}$$

where $\omega_f(k) = \eta_f k^2/\rho_f$, and we choose the branch cut of the square-root function to lie along the negative real axis. An analogous solution is found for $z < 0$. This demonstrates that the (in-plane) Fourier transforms of the bulk and membrane velocities are simply related,

$$\mathbf{v}_f(\mathbf{k},z,\omega) = \exp[-kz\sqrt{1 + i\omega/\omega_f(k)}]\mathbf{v}_m(\mathbf{k},\omega), \tag{A16}$$

where our Fourier transform convention is $f(\mathbf{k},\omega) = \int d^2r\, dt\, e^{-i(\mathbf{k}\cdot\mathbf{r}+\omega t)} f(\mathbf{r},t)$. We can then apply this to eliminate the fluid velocity from Eq. (A8),

$$\left.\frac{\partial\mathbf{v}_f(\mathbf{k},z,\omega)}{\partial z}\right|_{z=0} = -k\sqrt{1 - i\omega/\omega_f(k)}\,\mathbf{v}_m(\mathbf{k},\omega), \tag{A17}$$

which corresponds to the well-known limit of the body force from the bulk membrane [17,18] in the limit $\omega \to 0$. Fourier transforming Eq. (A8) in space, we get

$$i\omega\rho_m\mathbf{v}_m(\mathbf{k},\omega) = [-\eta_m(\omega)k^2 - 2\eta_f k\sqrt{1 + i\omega/\omega_f(k)}]\mathbf{v}_m + i\mathbf{k}P_m + \mathbf{f}(\mathbf{k},\omega). \tag{A18}$$

We apply the transverse projection operator, $P^{\perp}(k) = (\overleftrightarrow{I} - \frac{\mathbf{kk}}{k^2})$ as a simple way to eliminate the pressure, noting $P^{\perp}(k)\mathbf{v}_m(\mathbf{k},\omega) = \mathbf{v}_m(\mathbf{k},\omega)$ by the incompressibility requirement. Then,

$$i\omega\rho_m\mathbf{v}_m(\mathbf{k},\omega) = [-\eta_m(\omega)k^2 - 2\eta_f k\sqrt{1 + i\omega/\omega_f(k)}]\mathbf{v}_m + P^{\perp}(k)\mathbf{f}(\mathbf{k},\omega). \tag{A19}$$

This determines the membrane Oseen tensor, as defined in Eq. (1):

$$v_m^i(\mathbf{k},\omega) = T^{ij}(\mathbf{k},\omega)f^j(\mathbf{k},\omega), \tag{A20}$$

where the Einstein summation convention is assumed and

$$T^{ij}(\mathbf{k},\omega) = \frac{\delta_{ij} - k_i k_j/k^2}{i\omega\rho_m + \eta_m(\omega)k^2 + 2\eta_f k\sqrt{1 + i\omega/\omega_f(k)}}. \tag{A21}$$

Equation (3) reduces to the standard membrane Oseen tensor for a quasi-2D membrane [5,17] in the limit of $\omega \to 0$.

APPENDIX B: IMMERSED-BOUNDARY CALCULATION OF DRAG

In the immersed-boundary (IB) scheme, forces applied to particles are distributed over the particle's size using a

"finite delta function," $\delta_a(\mathbf{r})$, and the velocity of the particle related to the fluid velocity using that same δ function [31,32]. This technique has been used to calculate a wide variety of mobilities and related features, such as long-time tails, in three-dimensional fluids [32,34,35]. If we have a particle at position $\mathbf{R}_p$, in the IB scheme, its velocity is given by

$$\mathbf{V}_p = \int d^2r'\, \mathbf{v}_m(\mathbf{r}')\delta_a(\mathbf{R}_p - \mathbf{r}'). \tag{B1}$$

To account for a force $\mathbf{F}$ applied to an IB particle, we apply a force to the fluid:

$$\mathbf{f}_v(\mathbf{r},t) = \mathbf{F}(t)\delta_a(\mathbf{R}_p - \mathbf{r}'). \tag{B2}$$

This allows us to compute ζ simply in the immersed-boundary approximation. If we apply a force $\mathbf{F}(t) = \int \frac{d\omega}{2\pi} e^{i\omega t}\mathbf{F}(\omega)$, then we can calculate the fluid velocity using Eqs. (1) and (3). We assume for convenience that the force is sufficiently small that the particle does not travel far from the origin, and so we can take $\mathbf{R}_p \approx 0$, and thus

$$\mathbf{v}_m(\mathbf{k},\omega) = \overleftrightarrow{T}(\mathbf{k},\omega)\mathbf{f}_v(\mathbf{k},\omega) = \overleftrightarrow{T}(\mathbf{k},\omega)\delta_a(\mathbf{k})\mathbf{F}(\omega) \tag{B3}$$

and the particle velocity is, similarly,

$$\mathbf{V}_p(\omega) \approx \int d^2r'\, \mathbf{v}_m(\mathbf{r}',\omega)\delta_a(\mathbf{r}') \tag{B4}$$

$$= \int \frac{d^2k}{(2\pi)^2}\mathbf{v}_m(\mathbf{k},\omega)\delta_a(-\mathbf{k}) \tag{B5}$$

$$= \int \frac{d^2k}{(2\pi)^2}|\delta_a(\mathbf{k})|^2\, \overleftrightarrow{T}(\mathbf{k},\omega)\mathbf{F}(\omega). \tag{B6}$$

If we choose $\mathbf{F}$ to be in the x direction, we can simply perform the angular integration, allowing us to determine the mobility $\mu(\omega)$, where $\mathbf{V}_p(\omega) = \mu(\omega)\mathbf{F}(\omega)$, and $\zeta(\omega) = 1/\mu(\omega)$,

$$\mu(\omega) = \frac{1}{4\pi}\int_0^\infty dk \frac{k|\delta_a(\mathbf{k})|^2}{i\omega\rho_m + \eta_m k^2 + \eta_f k\sqrt{1 + i\omega/\omega_f(k)}}. \tag{B7}$$

$\delta_a(\mathbf{r})$ is usually chosen to have compact support, as well as other advantageous numerical properties [31], but as we are not using it for a simulation, we choose a Gaussian for analytical simplicity,

$$\delta_a(\mathbf{r}) = \frac{1}{\pi b^2}e^{-(r/b)^2}. \tag{B8}$$

Because of the inexactness of our immersed-boundary approximation, the Gaussian size b is not necessarily equal to the object radius a. We choose $b = \beta a$, which yields Eq. (6). β is fit such that the immersed-boundary mobility Eq. (6) best agrees with the Saffman-Delbrück-Hughes-Pailthorpe-White result [1,2,4] in the limit of a purely viscous membrane ($\omega = 0$). This yields $\beta = 0.797\,91$. A comparison between the immersed-boundary approximation and the complete result is provided in Fig. 9.

The long-time tail can also be extracted from the immersed-boundary approximation by using Eq. (6). We can write the equation of motion for an embedded particle with drag $\zeta(\omega)$:

$$i\omega M\mathbf{V}_p(\omega) = -\zeta(\omega)\mathbf{V}_p(\omega), \tag{B9}$$

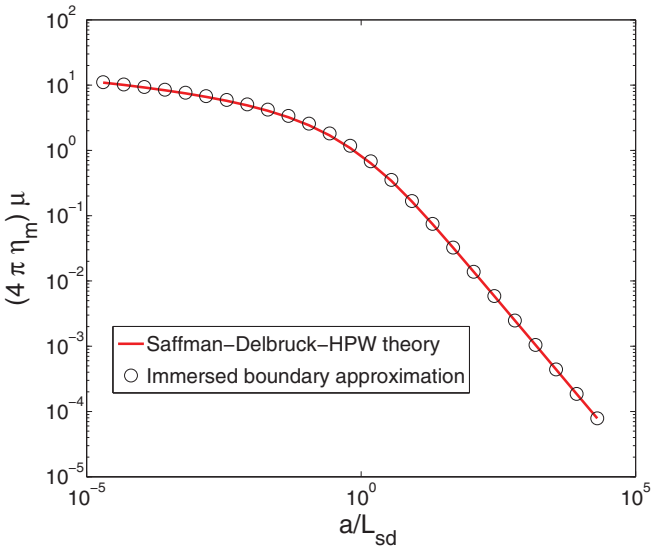

FIG. 9. (Color online) Comparison of the Saffman-Delbrück-Hughes-Pailthorpe-White result with numerical evaluation of Eq. (6) with $\beta = 0.797\,91$. The immersed-boundary approximation is an excellent approximation over ten decades of a/L_{sd}, with a maximum deviation of 8%.

where M is the particle mass. This represents the motion of a particle with a time-dependent drag, as becomes obvious if we invert the Fourier transform:

$$M\frac{d}{dt}\mathbf{V}_p(t) = -\int_{-\infty}^{t}\zeta(t-t')\mathbf{V}_p(t'). \tag{B10}$$

Moving to Laplace transform space, we can calculate the correlation function as in Sec. III above,

$$\langle \mathbf{V}_p(t_0+t)\cdot\mathbf{V}_p(t_0)\rangle = \int_{\delta-i\infty}^{\delta+i\infty}\frac{ds}{2\pi i}\, e^{st}\frac{M}{Ms + \hat{\zeta}(s)}\langle|\mathbf{V}_p|^2\rangle. \tag{B11}$$

We will see later that the long-time limit is controlled by the integrand's asymptotic behavior as $s \to 0$, and that $\hat{\zeta}(s) \sim s^{1/2}$, so we drop the mass term. We then obtain

$$\langle \mathbf{V}_p(t_0+t)\cdot\mathbf{V}_p(t_0)\rangle \approx 2k_BT\int_{\delta-i\infty}^{\delta+i\infty}\frac{ds}{2\pi i}\, e^{st}\hat{\zeta}^{-1}(s), \tag{B12}$$

where

$$\zeta^{-1}(s) = \frac{1}{4\pi}\int_0^\infty dk \frac{ke^{-\beta^2k^2a^2/2}}{s\rho_m + \eta_m k^2 + 2\eta_f k\sqrt{1 + s/\omega_f}}. \tag{B13}$$

We can then exchange integrals and integrate along the branch cut, exactly as in Sec. III:

$$\langle \mathbf{V}_p(t_0+t)\cdot\mathbf{V}_p(t_0)\rangle = \frac{k_BT}{\pi^2}\int_0^\infty dx\int_0^\infty dk\, e^{-[x+\omega_f(k)]t}e^{-\beta^2k^2a^2/2} \times \frac{k^2\eta_f\sqrt{x/\omega_f}}{(\eta_m k^2 - \rho_m\omega_f - \rho_m x)^2 + (2k\eta_f)^2x/\omega_f}. \tag{B14}$$

Integrating, we find for the long-time limit,

$$\langle \mathbf{V}_p(t_0+t)\cdot\mathbf{V}_p(t_0)\rangle = \frac{k_BT}{8\pi\eta_f}\sqrt{\frac{\rho_f}{\pi\eta_f}}t^{-3/2}. \quad \text{(B15)}$$

So the $t^{-3/2}$ long-time tail is also present for the diffusion of an embedded particle, at least in the immersed-boundary approximation.

APPENDIX C: OTHER MOBILITY APPROXIMATIONS

We have chosen to describe the mobility of a particle embedded within a membrane by using the immersed-boundary approximation. To ensure that this approximation does not create an unphysical new behavior, we compare it with other schemes for approximating the mobility.

Levine and Lubensky applied both "shell localization" and "volume localization" to determine drag coefficients from response functions in [33], and they showed that these schemes reproduce the correct low-frequency limit of the drag coefficient in three-dimensional fluids. The localization approximations are similar in spirit to the immersed-boundary approach. Instead of averaging over the fluid flow near the particle, as in the IB scheme Eq. (B1), the localization schemes assume the particle follows the fluid precisely, i.e., $\delta_a(\mathbf{r}) \to \delta(\mathbf{r})$:

$$\mathbf{V}_p = \mathbf{v}_m(\mathbf{R}_p). \quad \text{(C1)}$$

The localization schemes then assume that a force $\mathbf{F}(t)$ applied to the particle results in a force on the fluid $\mathbf{f}_v(\mathbf{k},\omega)$,

$$\mathbf{f}_v(\mathbf{k},\omega) = \mathbf{F}(\omega)\mathcal{F}(k). \quad \text{(C2)}$$

Assuming the particle's deviations from the origin are small, then

$$\mathbf{V}_p(\omega) = \int \frac{d^2k}{(2\pi)^2}\mathbf{v}_m(\mathbf{k},\omega). \quad \text{(C3)}$$

The membrane velocity can then be determined by Eqs. (1) and (C2). Performing the angular integral, we find $\mathbf{V}_p(\omega) = \mu(\omega)\mathbf{F}(\omega)$, where

$$\mu(\omega) = \frac{1}{4\pi}\int_0^\infty dk \frac{k\mathcal{F}(k)}{i\omega\rho_m + \eta_m k^2 + \eta_f k\sqrt{1+i\omega/\omega_f(k)}}. \quad \text{(C4)}$$

The "shell" and "volume" localization schemes are simply physically motivated assumptions for the form $\mathcal{F}(k)$. Volume localization would set a simple cutoff at $k_{\max} = \pi/2a$; however, this choice causes Eq. (C4) to diverge at $\omega = 0$. Shell localization assumes that the force is localized at the disk surface, i.e., $\mathbf{f}_v(\mathbf{r},t) = \mathbf{F}(t)\delta(r-a)/(2\pi a)$ or $\mathcal{F}(k) = J_0(ka)$, where J_0 is a Bessel function of the first kind.

For a purely viscous membrane at zero frequency, the shell localization provides a reasonable approximation to the Saffman-Delbrück-Hughes-Pailthorpe-White result (Fig. 10). The quality of this approximation could potentially be improved by including an effective shell size, as in the immersed-boundary approximation. We prefer the IB scheme as it treats the coarse-graining of the force applied to the particle and the force applied by the particle on the fluid in a symmetric manner. The quasi-2D IB scheme is also amenable to stochastic numerical solution [6,73] as in [32].

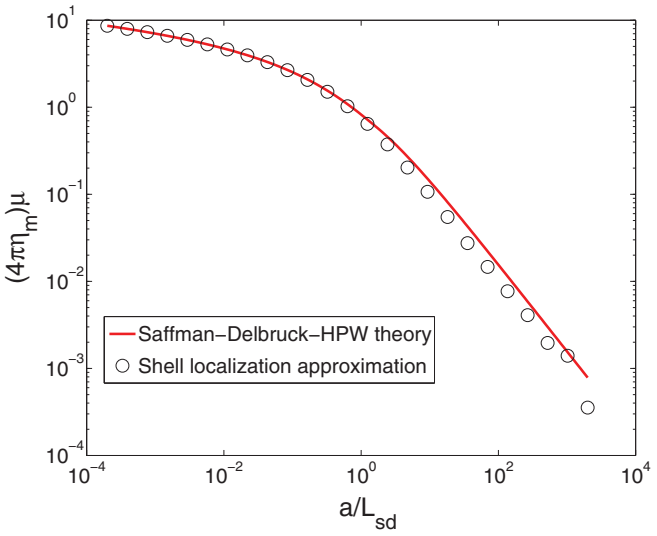

FIG. 10. (Color online) Comparison of the Saffman-Delbrück-Hughes-Pailthorpe-White result with numerical evaluation of Eq. (C4). The shell localization approximation is an excellent approximation for $a \ll L_{sd}$, but is systematically low at $a > L_{sd}$; these deviations are ~30%; there are also oscillations at large a/L_{sd}.

There is also a known exact result for the mobility of a fluid domain of surface viscosity η_m in a membrane of equal viscosity [74],

$$\zeta_{\text{DeKoker}} = \pi\left[\int_0^\infty dx \frac{J_1(x)^2}{x^2(\eta_m x + 2\eta_f a)}\right]^{-1}. \quad \text{(C5)}$$

If we apply the viscous-viscoelastic correspondence to this result, we can extend it to a complex, frequency-dependent surface viscosity $\eta_m(\omega)$.

Regardless of whether we use the immersed-boundary drag Eq. (6), the shell-localization scheme Eq. (C4), or the fluid domain exact result Eq. (C5), we still see the same qualitative picture of the effective 3D shear modulus $G_{3D}(\omega)$. The various schemes are plotted in Fig. 11 for the Maxwell model as above. All show the Maxwell behavior at low frequencies, but a crossover to viscous behavior dominated by the outside fluid at large frequencies. In most cases, there is reasonable quantitative agreement, except for the known problem with the shell localization scheme at high frequencies.

APPENDIX D: DOMAIN FLICKERING IN A MAXWELL MODEL MEMBRANE

We can calculate many interesting features of domain flickering exactly if we assume that the membrane's viscoelastic parameters are set by a simple Maxwell model, which assumes a single relaxation time, τ_c, for the stress, i.e.,

$$\eta_m(\omega) = \frac{\eta_0}{1+i\omega\tau_c}, \quad \text{(D1)}$$

where τ_c^{-1} is the crossover frequency. One clear consequence of this form is that $|\eta_m(\omega)|$ decreases significantly for frequencies $\omega \gg \tau_c^{-1}$. This means that at large frequencies, the relaxation rate will be controlled by the bulk fluid viscosity, η_f,

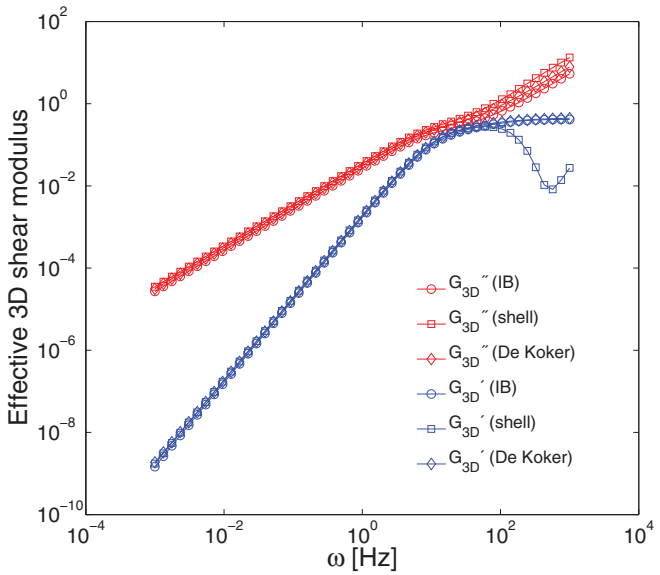

FIG. 11. (Color online) Other approximation schemes are consistent with the immersed-boundary approximation.

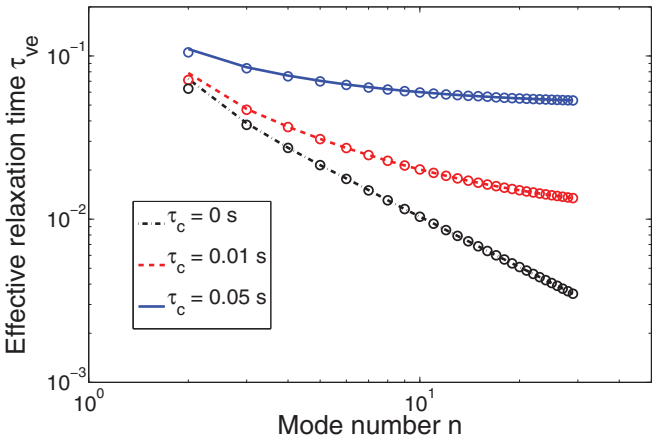

FIG. 12. (Color online) Effective viscoelastic relaxation times τ_{ve} for domain relaxation in a Maxwell-model membrane [Eq. (D10)]. τ_{ve} goes to a constant value for large n ($\tau_n \ll \tau_c$). For this figure, $R = 1\ \mu$m, $\eta_m = 5 \times 10^{-6}$ poise cm, and $\sigma = 0.2$ pN. Open circles are extracted from numerical evaluation of the correlation function, as in Fig. 13. Deviations at $n = 2$ indicate the breakdown of the approximation Eq. (D8).

and not the membrane surface viscosity $\eta_m(\omega)$. For parameters typical to [16], the integrand in Eq. (13) is large only up to $x_c \sim 10$; therefore, if $|\eta_m(\omega)|x_c \ll 2\eta_f R$, the function $\gamma_n(\omega)$ is dominated by the bulk fluid contribution, and the decay rate is just given by the Stone-McConnell [9] result, which neglects membrane response altogether,

$$\gamma_n^{-1}(\omega) \to \tau_n^{\text{bulk}} = \frac{2\pi R^2 \eta_f}{\sigma} \frac{n^2 - 1/4}{n^2(n^2-1)}. \tag{D2}$$

This is independent of membrane viscosity, and hence is frequency-independent. We will see that this high-frequency behavior determines the short-time correlation function,

$$\langle u_n(t) u_n^*(t')\rangle = \langle |u_n|^2\rangle e^{-|t-t'|/\tau_n^{\text{bulk}}} \quad \text{for} \quad t \ll \frac{2\eta_f R}{\eta_0}\tau_c x_c. \tag{D3}$$

We can also look at the long-time behavior of the correlation function. We can extract the correlation function of u_n from Eqs. (10) and (11) via the Wiener-Khinchin theorem:

$$\langle u_n(t) u_n^*(t')\rangle = \frac{\langle |u_n|^2\rangle}{\pi} \int d\omega \frac{\text{Re}\{\gamma_n(\omega)\}}{|i\omega + \gamma_n(\omega)|^2} e^{i\omega(t-t')}. \tag{D4}$$

If the function $\gamma_n(\omega)$ is frequency-independent, e.g., $\gamma_n(\omega) = \tau_n^{-1}$ for a purely viscous membrane, we obtain the usual fluctuation-dissipation result from Eq. (D4), $\langle u_n(t) u_n^*(t')\rangle = \langle |u_n|^2\rangle \exp(-|t-t'|/\tau_n)$.

Using causality, we find that Eq. (D4) reduces to ($t > 0$) [38]

$$\langle u_n(t) u_n^*(0)\rangle = \frac{\langle |u_n|^2\rangle}{\pi} \int_{-\infty - i\epsilon}^{\infty - i\epsilon} d\omega \frac{1}{i\omega + \gamma_n(\omega)} e^{i\omega t}, \tag{D5}$$

where ϵ is a positive infinitesimal. This equation can be evaluated using the residue theorem, extending the contour into the upper half-plane,

$$\langle u_n(t) u_n^*(0)\rangle = \langle |u_n|^2\rangle 2i \sum_k \text{Res}\left(\frac{1}{i\omega + \gamma_n(\omega)} e^{i\omega t}; \omega_k\right), \tag{D6}$$

where the sum is over the poles ω_k with $i\omega_k + \gamma_n(\omega_k) = 0$ in the upper half-plane. The long-time behavior of this correlation function is set by the slowest decay, i.e., the pole ω_k with the

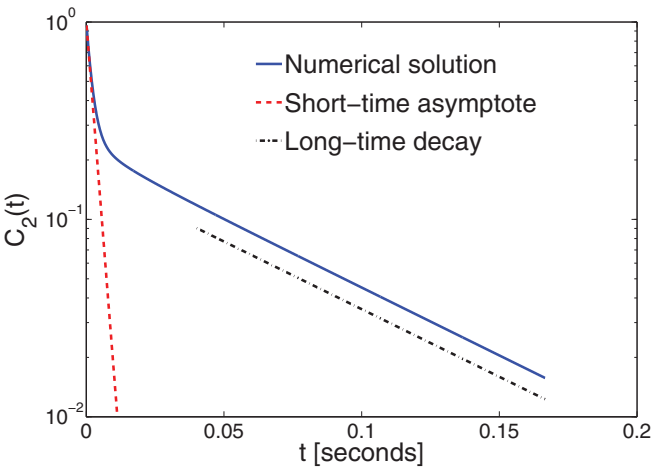

FIG. 13. (Color online) Autocorrelation function $C_n(t) \equiv \langle u_n(t) u_n^*(0)\rangle / \langle |u_n|^2\rangle$ for domain fluctuations in a Maxwell-model membrane; parameters chosen are $\eta_m = 5 \times 10^{-6}$ poise cm, $\eta_f = 0.01$ poise, $\sigma = 0.8$ pN, $R = 1\ \mu$m, $\tau_c = 0.05$ s, $n = 2$. The data are well described by a short-time exponential decay of $\tau^{\text{bulk}} = 2.5$ ms [set by Eq. (D2)] and a long-time asymptote given by $\tau_{ve} = 0.063$ s [set by Eq. (D10)]. The exact solution is found by numerically evaluating Eq. (D4) with $\gamma_n(\omega)$ given by Eq. (13).

smallest (positive) imaginary part. This is a difficult problem to solve, but it can be treated in the limit of $2\eta_f R/\eta_m(0) \ll 1$.

In the limit of a purely two-dimensional membrane, $\eta_f = 0$, we can evaluate the integral in Eq. (13), finding

$$\gamma_n^{2D}(\omega) = \frac{n\sigma}{4R\eta_m(\omega)}. \tag{D7}$$

There is then only one pole in Eq. (D6), at $\omega_k = i\gamma_n^{2D}(0)/[1 + \tau_c\gamma_n^{2D}(0)]$, corresponding to long-time exponential decay with decay time $\tau_{ve}^{2D} = \tau_c + 1/\gamma_n^{2D}(0)$. This implies that at large mode numbers n, the viscoelastic relaxation time does not decay to zero, but rather to a saturation value given by the crossover time scale τ_c; this feature is preserved in the full quasi-2D limit.

The 2D decay rate above corresponds to the $\Lambda = 0$ term in the expansion of Eq. (13), where $\Lambda = 2\eta_f R/\eta_m(0)$; at first order,

$$\gamma_n(\omega) \approx \frac{n\sigma}{4R\eta_m(\omega)} - \frac{4n^2(n^2-1)\eta_f\sigma}{3\pi\eta_m(\omega)^2}\frac{\Gamma(n-3/2)}{\Gamma(n+5/2)} \tag{D8}$$

$$\equiv A_n(1 + i\omega\tau_c) - B_n(1 + i\omega\tau_c)^2, \tag{D9}$$

where $A_n = \gamma_n^{2D}(0)$ and $B_n = \frac{4n^2(n^2-1)\eta_f\sigma}{3\pi\eta_m(0)^2}\frac{\Gamma(n-3/2)}{\Gamma(n+5/2)}$. This is an asymptotic approximation in small Λ/n, and is correct in the limit of small domains, large membrane viscosities, and large n. Thus, for Eq. (D8) to approximate Eq. (13) well, we must have $B_n \ll A_n$; this allows us to identify the root of the quadratic equation that lies in the upper half-plane, leading to

$$\tau_{ve} \approx \frac{2B_n\tau_c^2}{\sqrt{(1 + A_n\tau_c)^2 - 4B_n\tau_c} - (1 + A_n\tau_c - 2B_n\tau_c)}. \tag{D10}$$

Once again, we can see that if the zero-frequency relaxation time is small compared with τ_c, the viscoelastic domain will relax with a time scale $\tau_{ve} \to \tau_c$ (Fig. 12).

To confirm our analysis, we numerically evaluate the correlation function $\langle u_n(t)u_n^*(t')\rangle$ by using Eqs. (13), (D4), and (D1). The small-time behavior is most easily seen in systems with large τ_c compared to the short-time decay τ_n^{bulk}; this is illustrated in Fig. 13. The numerical solution is well-fit to a double-exponential form, $C_n(t) \equiv \langle u_n(t' + t)u_n^*(t')\rangle/\langle|u_n|^2\rangle = \frac{1}{1+\beta}(e^{-t/\tau_1} + \beta e^{-t/\tau_2})$. We find, as expected, that at short times we get exponential decay with time constant τ_n^{bulk}, and at long times there is exponential decay with time constant τ_n [from Eq. (8)] if $\tau_n \gg \tau_c$, and with a time constant $\tau_{ve} \sim \tau_c$ if $\tau_c \gg \tau_n$ (Figs. 12 and 13).

[1] P. G. Saffman and M. Delbrück, Proc. Natl. Acad. Sci. (USA) **72**, 3111 (1975).
[2] B. D. Hughes, B. A. Pailthorpe, and L. R. White, J. Fluid Mech. **110**, 349 (1981).
[3] P. Cicuta, S. L. Keller, and S. L. Veatch, J. Phys. Chem. B **111**, 3328 (2007).
[4] E. P. Petrov and P. Schwille, Biophys. J. **94**, L41 (2009).
[5] N. Oppenheimer and H. Diamant, Biophys. J. **96**, 3041 (2009).
[6] B. A. Camley and F. L. H. Brown, Phys. Rev. Lett. **105**, 148102 (2010).
[7] V. Prasad, S. A. Koehler, and E. R. Weeks, Phys. Rev. Lett. **97**, 176001 (2006).
[8] J. C. Alexander, A. J. Bernoff, E. K. Mann, J. A. Mann, J. R. Wintersmith, and L. Zou, J. Fluid Mech. **571**, 191 (2007).
[9] H. A. Stone and H. M. McConnell, Proc. R. Soc. London, Ser. A **448**, 97 (1995).
[10] Z. H. Nguyen, M. Atkinson, C. S. Park, J. Maclennan, M. Glaser, and N. Clark, Phys. Rev. Lett. **105**, 268304 (2010).
[11] C. W. Harland, M. J. Bradley, and R. Parthasarathy, Proc. Natl. Acad. Sci. (USA) **107**, 19146 (2010).
[12] R. E. Waugh, Biophys. J. **19**, 19 (1982).
[13] G. Crawford and J. Earnshaw, Biophys. J. **52**, 87 (1987).
[14] R. Dimova, B. Pouligny, and C. Dietrich, Biophys. J. **79**, 340 (2000).
[15] C. Esposito *et al.*, Biophys. J. **93**, 3169 (2007).
[16] B. A. Camley, C. Esposito, T. Baumgart, and F. L. H. Brown, Biophys. J. **99**, L44 (2010).
[17] D. K. Lubensky and R. E. Goldstein, Phys. Fluids **8**, 843 (1996).
[18] A. J. Levine and F. C. MacKintosh, Phys. Rev. E **66**, 061606 (2002).
[19] K. Xu, M. G. Forest, and I. Klapper, J. Non-Newton. Fluid Mech. **145**, 150 (2007).
[20] T. M. Squires and T. G. Mason, Annu. Rev. Fluid Mech. **42**, 413 (2010).
[21] H. Deuling and W. Helfrich, J. Phys. (France) **37**, 1335 (1976).
[22] U. Seifert, Adv. Phys. **46**, 13 (1997).
[23] W. Helfrich, Eur. Phys. J. B **1**, 481 (1998).
[24] F. L. Brown, Annu. Rev. Phys. Chem. **59**, 685 (2008).
[25] F. Brochard and J. Lennon, J. Phys. (France) **36**, 1035 (1975).
[26] L. C.-L. Lin and F. L. H. Brown, Phys. Rev. Lett. **93**, 256001 (2004).
[27] L. C.-L. Lin and F. L. H. Brown, Phys. Rev. E **72**, 011910 (2005).
[28] A. Serra and J. M. Rubí, Physica A **142**, 342 (1987).
[29] M. Doi and S. F. Edwards, *The Theory of Polymer Dynamics* (Clarendon, Oxford, 1999).
[30] T. G. Mason, Rheol. Acta **39**, 371 (2000).
[31] C. Peskin, Acta Numer. **11**, 1 (2002).
[32] P. J. Atzberger, P. R. Kramer, and C. S. Peskin, J. Comput. Phys. **224**, 1255 (2007).
[33] A. J. Levine and T. C. Lubensky, Phys. Rev. E **63**, 041510 (2001).
[34] P. J. Atzberger, J. Comput. Phys. **230**, 2821 (2011).
[35] P. J. Atzberger, Phys. Lett. A **351**, 225 (2006).
[36] The authors of [11] have recently informed us of experimental artifacts that significantly affect their conclusions on the viscoelasticity of lipid bilayers. [R. Parthasarathy (personal communication, June 2011)].
[37] Using the 3D formula may, however, extract the correct qualitative picture if the bulk viscosity is small. More precisely, if the probe size a and frequency ω are such that $a \ll L_{sd}(\omega)$, Eq. (6) shows that $\zeta \sim \eta_m(\omega)$ up to logarithmic corrections. If this is the case, then G_{3D} is proportional to G_{2D}/a, and there is a simple correspondence between the analysis of [11] and the underlying membrane viscosity.

[38] R. Kubo, M. Toda, and N. Hashitsume, *Statistical Physics II*, 2nd ed. (Springer-Verlag, Berlin, 1991).
[39] N. G. Van Kampen, *Stochastic Processes in Physics and Chemistry* (North Holland, Amsterdam, 2007).
[40] P. M. Chaikin and T. C. Lubensky, *Principles of Condensed Matter Physics* (Cambridge University Press, Cambridge, UK, 2000).
[41] B. Alder and T. Wainwright, Phys. Rev. A **1**, 18 (1970).
[42] D. A. Weitz, D. J. Pine, P. N. Pusey, and R. J. A. Tough, Phys. Rev. Lett. **63**, 1747 (1989).
[43] R. Zwanzig, *Nonequilibrium Statistical Mechanics* (Oxford University Press, New York, 2001).
[44] R. Zwanzig and M. Bixon, Phys. Rev. A **2**, 2005 (1970).
[45] E. Hinch, J. Fluid Mech. **72**, 499 (1975).
[46] J. Happel and H. Brenner, *Low Reynolds Number Hydrodynamics* (Kluwer, The Hague, 1983).
[47] J.-P. Hansen and I. R. McDonald, *Theory of Simple Liquids*, 3rd ed. (Academic, The Netherlands, 2006).
[48] L. Reichl, *A Modern Course in Statistical Physics* (Wiley-Interscience, New York, 1998).
[49] S. Ramachandran, S. Komura, and G. Gompper, Europhys. Lett. **89**, 56001 (2010).
[50] M. A. van der Hoef and D. Frenkel, Phys. Rev. A **41**, 4277 (1990).
[51] T. B. Liverpool and F. C. MacKintosh, Phys. Rev. Lett. **95**, 208303 (2005).
[52] J. Wohlert and O. Edholm, J. Chem. Phys. **125**, 204703 (2006).
[53] K. Seki and S. Komura, Phys. Rev. E **47**, 2377 (1993).
[54] N. Oppenheimer and H. Diamant, Phys. Rev. E **82**, 041912 (2010).
[55] R. G. Larson, *The Structure and Rheology of Complex Fluids* (Oxford University Press, New York, 1999).
[56] S. L. Veatch and S. L. Keller, Biochim. Biophys. Acta **1746**, 172 (2005).
[57] N. Kahya, D. Scherfeld, K. Bacia, B. Poolman, and P. Schwilla, J. Biol. Chem. **278**, 28109 (2003).
[58] T. Baumgart, S. Das, W. Webb, and J. Jenkins, Biophys. J. **89**, 1067 (2005).
[59] G. Espinosa, I. López-Montero, F. Monroy, and D. Langevin, Proc. Natl. Acad. Sci. (USA) **108**, 6008 (2011).
[60] E. K. Mann, S. Hénon, D. Langevin, J. Meunier, and L. Léger, Phys. Rev. E **51**, 5708 (1995).
[61] A. J. Wagner and M. E. Cates, Europhys. Lett. **56**, 556 (2001).
[62] H. Furukawa, Phys. Rev. E **61**, 1423 (2000).
[63] A. J. Bray, Adv. Phys. **43**, 357 (1994).
[64] J. Fan, T. Han, and M. Haataja, J. Chem. Phys. **133**, 235101 (2010).
[65] Y. Tserkovnyak and D. R. Nelson, Proc. Natl. Acad. Sci. (USA) **103**, 15002 (2006).
[66] S. Ramadurai *et al.*, J. Am. Chem. Soc. **131**, 12650 (2009).
[67] Y. Gambin, R. Lopez-Esparza, M. Reffay, E. Sierecki, N. S. Gov, M. Genest, R. S. Hodes, and W. Urbach, Proc. Natl. Acad. Sci. (USA) **103**, 2098 (2006).
[68] A. Naji, A. J. Levine, and P. Pincus, Biophys. J. **93**, L49 (2007).
[69] A. Naji, P. J. Atzberger, and F. L. H. Brown, Phys. Rev. Lett. **102**, 138102 (2009).
[70] A. J. Levine and T. C. Lubensky, Phys. Rev. E **65**, 011501 (2001).
[71] R. Granek, Soft Matter **7**, 5281 (2011).
[72] R. B. Bird and O. Hassager, *Dynamics of Polymeric Liquids*, Vol. 1 (Wiley Interscience, New York, 1987).
[73] B. Camley, P. Atzberger, and F. Brown (unpublished).
[74] R. DeKoker, Ph.D. thesis, Stanford University (1996).